Journal of Materials Chemistry C

Accepted Manuscript

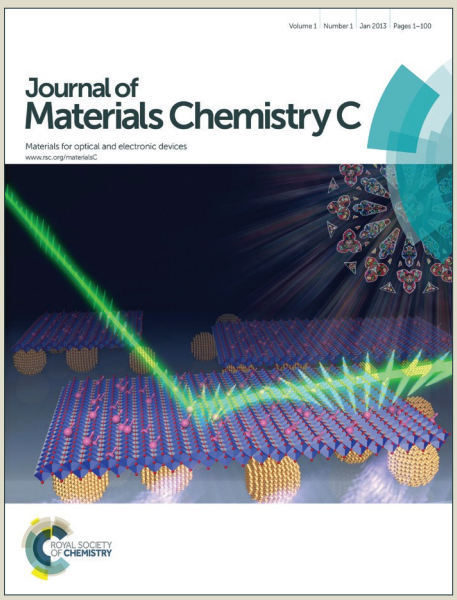

ROYAL SOCIETY OF CHEMISTRY

www.rsc.org/materialsC

Journal of Materials Chemistry C

Cite this: DOI: 10.1039/c0xx00000x

PAPER

www.rsc.org/xxxxxx

Interplay between local environments and photoluminescence of Eu^{2+} in $Ba_2Zr_2Si_3O_{12}$: blue shift emission, optimal bond valence and luminescence mechanisms

Yang Zhang, [a, b] Xuejiao Li, [a, b] Kai Li, [a,b] Hongzhou Lian, [a] Mengmeng Shang, [a] and Jun Lin [a,*]

Received (in XXX, XXX) Xth XXXXXXXXX 201X, Accepted Xth XXXXXXXXX 201X
DOI: 10.1039/b000000x

$Ba_{2(1-x)}Zr_2Si_3O_{12}$ (BZSO): xEu^{2+} (x = 0.005-0.06) phosphors have been prepared by high temperature solid state reaction. By X-ray powder diffraction, the structural properties including phase purity were analyzed through Rietveld analysis. The BZSO: Eu^{2+} phosphors exhibit broad excitation band ranging from 200 to 450 nm, and an intense asymmetric green emission band centered at 501 nm under excitation of 365 nm. The optimum doping concentration of Eu^{2+} was found for x = 0.03. The detailed energy transfer mechanism among Eu^{2+} in BZSO is found to be dipole–dipole mechanism, and the critical distance (R_C) for Eu^{2+} ions calculated by the concentration quenching and spectral overlap methods are 20.45 and 25.83 Å, respectively. Furthermore, the unexpected blue shift (from green to cyan) in emission and the increase on the thermal quenching barrier upon cation substitutions (Ca^{2+}/Sr^{2+} for Ba^{2+}) in BZSO: 0.03Eu^{2+} system have been investigated, which is due to the variation of the crystal field strength that the 5d orbital of Eu^{2+} ion experiences. The underlying mechanism is ascribed to the differences between the average structure and the local coordination environments on activator ions (Eu^{2+}), as confirmed by the refinement results. Considering the merits of near-UV light excitation, broad band emission, and good thermal stability, these materials have potential application as WLEDs phosphors.

1. Introduction

Over the decades, white light emitting diodes (WLEDs), as one promising solid-state lighting sources, has aroused another revolution to overtake conventional incandescent or fluorescence lamps on the illumination, considering their fascinating advantages such as energy savings, small size, eco-friendliness, high brightness and a long lifetime.[1-10] Recently, most of commercial lamps combine the blue InGaN chip with a yellow-emitting $Y_3Al_5O_{12}$: Ce^{3+} (YAG: Ce^{3+}) garnet-based phosphor to obtain white light. Unfortunately, the drawbacks of this method are low color rendering index (CRI < 75) due to the lack of red component and the corresponding high correlated color temperature (CCT), which makes such devices undesirable for indoor use.[2, 11-14] An alternative strategy to obtain white light with high CRI may be based on a combination of a near ultraviolet (NUV) LED chip (365-410 nm) with red, green, and blue emitting phosphors. However, the bottleneck of this method is the scarcity of efficient phosphors, owing to the large Stokes shift between excitation and emission in the NUV excitable phosphor.[15, 16] Therefore, it is vital to develop some novel phosphors with high stability, high efficiency and ultrasensitivity in NUV region from the practical viewpoint.[5, 17, 18]

Eu^{2+} ion, as one of the most widely used activator in phosphors, has broad excitation band covering the emissions from NUV LED chips and an emission band ranging from the blue region to the red region due to the parity-allowed 4f-5d transitions.[19-22] Because the 5d orbitals of Eu^{2+} are sensitive to the surrounding crystal field and strongly affected by the polarizability of the host crystal, thus, the excitation and emission energies are tunable in a wide range through modulate the host composition and crystal structure.[5, 23, 24] On the other hand, silicate-based phosphors have attracted much attention due to their structural diversity, visible light transparency, higher thermal stability and relatively easy preparation.[25-27] Thus, in this study, we report a green emitting $Ba_2Zr_2Si_3O_{12}$ (BZSO) phosphor host doped with Eu^{2+}, which is formed from the framework of ZrO_6 octahedras and SiO_4 tetrahedras sharing vertexes.[28- 30] This sample presents an intense broad excitation band from 200 to 450 nm which overlaps with the emission of the NUV LED chip, while a broad asymmetric emission band peaking at 501 nm is obtained under 365 nm excitation. There are two different emission centers (Eu^{2+}) in the crystal structure of BZSO: Eu^{2+}, confirmed by the Rietveld refinement analysis. Meanwhile, the detailed energy transfer mechanism among Eu^{2+} and the critical distance (R_C) for Eu^{2+} have been clarified in detail. In addition, an abnormal blue shift in emission is found in BZSO: 0.03Eu^{2+} with gradual substitution of Ba^{2+} with smaller Ca^{2+}/Sr^{2+}, accompanied by better thermal stability from Ca^{2+} to Sr^{2+}, then to Ba^{2+} for BZSO: 0.03Eu^{2+}. The underlying mechanism has been revealed to be the differences between the average structure and the local coordination environments on Eu^{2+} ions, which may significantly contribute for exploring novel phosphors in future research.

2. Expermental

2.1 Materials

$BaCO_3$, $SrCO_3$, $CaCO_3$, ZrO_2 and SiO_2 were purchased from Beijing Chemical Company. The Eu_2O_3 (99.999%) was purchased from Science and Technology Parent Company of Changchun Institute of Applied Chemistry. All chemicals were used directly without further purification.

2.2 Preparation

A series of $Ba_{2(1-x)}Zr_2Si_3O_{12}$ (BZSO): xEu^{2+} (x = 0.005-0.06) powder samples were prepared by conventional solid state reaction process. Firstly, the stoichiometry contents of $BaCO_3$, Eu_2O_3, ZrO_2 and SiO_2 with the purity higher than 99.99% were ground in an agate mortar for 45 min for a good mixing. The mixture was calcined in aluminum oxide crucible at 1200 ^oC for 4 h under a reducing atmosphere of N_2 (90%) and H_2 (10%). The sintered samples were grounded for 30 min to form a homogeneous mixture. Then, the mixture was fired again at 1400-1500 ^oC for 6 h under a reducing atmosphere of N_2 (90%) and H_2 (10%), yielding the resulting phosphors.

2.3 Characterization

The X-ray diffraction (XRD) patterns were performed on a D8 Focus diffractometer in the 2θ range from 10° to 100° operating at 40 kV and 40 mA with graphite-monochromatized Cu $K\alpha$ radiation (λ = 0.15405 nm). The Rietveld analysis of the XRD was done using the General Structure Analysis System (GSAS) program.[31] The photoluminescence (PL) measurements were recorded with a Hitachi F-7000 spectrophotometer equipped with a 150 W xenon lamp as the excitation source. The luminescence decay curves were obtained from a Lecroy Wave Runner 6100 Digital Osilloscope (1 GHz) using a tunable laser (pulse width = 4 ns, gate = 50 ns) as the excitation source (Contimuum Sunlite OPO). The temperature-dependent properties of the phosphors were measured with a Horiba-Jobin-Yvon Fluorolog-3 FL3-211 spectrometer equipped with a 450 W xenon lamp as the excitation source. All the measurements were performed at room temperature (RT).

3. Results and discussion

The XRD pattern of the $Ba_2Zr_2Si_3O_{12}$: $0.03Eu^{2+}$ (BZSO: $0.03Eu^{2+}$) sample was first defined by Rietveld refinement implemented with the structure model, which was built with crystal structure information identified by previous reports.[28, 29, 31] The observed, calculated, and the difference patterns of the XRD refinement of BZSO: $0.03Eu^{2+}$ is shown in Fig. 1a. The final refinement converged with weighted profiles of R_p= 6.05% and R_{wp} = 7.76%, thus ensuring the phase purity of the sample. As the crystallographic data of BZSO: $0.03Eu^{2+}$ shown in Table S1, this compound exhibits a cubic crystal system with space group $P2_13$ (No. 198), Z = 4, and its cell parameter is a = b = c = 10.24278 Å, V = 1074.62 $Å^3$, basically agreeing well with previous literatures.[28, 32] In the typical crystal structure of BZSO as displayed in Fig. 1b, two Zr atoms occupy only the 4a site coordinated by six O atoms to form two kinds of ZrO_6 octahedra. The Si atom forms SiO_4 tetrahedra with the occupation of 12b site. The three-dimensional structure of BZSO is formed from the framework of ZrO_6 octahedra and SiO_4 tetrahedra sharing the O^{2-} vertexes.[32] Notably, there are two distinctive Ba atoms with different coordination numbers as depicted in Fig. 1b. The Ba(1)

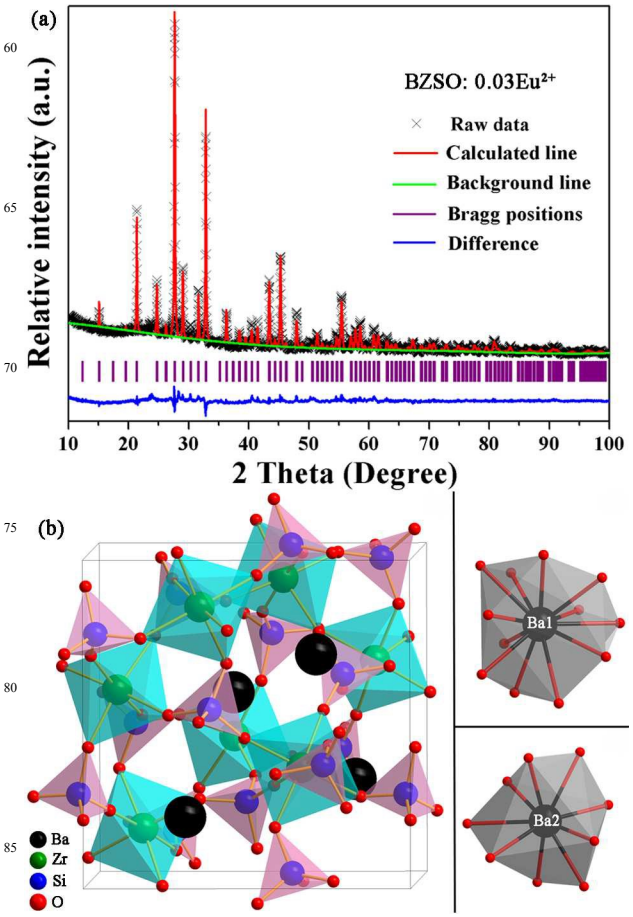

Fig. 1 (a) Experimental (cross), calculated (solid line), and difference (bottom) results of powder X-ray diffraction (XRD) refinements of $Ba_2Zr_2Si_3O_{12}$: $0.03Eu^{2+}$. Bragg reflections are indicated with tick marks. (b) Crystal structure representation of $Ba_2Zr_2Si_3O_{12}$ and the two different Ba^{2+} sites are depicted with twelve- and nine-coordination by oxygen atoms, respectively.

and Ba(2) atom both occupy the 4a site in the center of BaO_{12} polyhedron (CN = 12) and BaO_9 polyhedron (CN = 9), respectively. Considering the similar ionic radii and valence, the Eu^{2+} ions are expected to dissolve in the host by randomly occupying the Ba^{2+} sites.[33]

As shown in Fig. 2, the fine structure of BZSO: $0.03Eu^{2+}$ is further examined by high resolution transmission electron microscopy (HRTEM). It is obvious that the particles have smooth morphology with diameters in the scale of microns. The selected area electron diffraction (SAED) pattern in Fig. 2b presents strong concentric ring patterns that can be indexed to the (310), (311), (421) and (520) planes of BZSO, respectively, indicating the polycrystalline nature of the sample. It can be seen that continuous lattice fringes with a d spacing of 0.308 nm correspond to the distance of the (311) plane of BZSO in Fig. 2c, which is consistent with the results of SAED.

Fig. 3a depicts the photoluminescence excitation (PLE) and

emission (PL) spectra of BZSO: 0.03Eu^{2+} sample. The observed excitation spectrum consists of three absorption bands peaking at 272 nm, 331 nm and 370 nm, which can be attributed

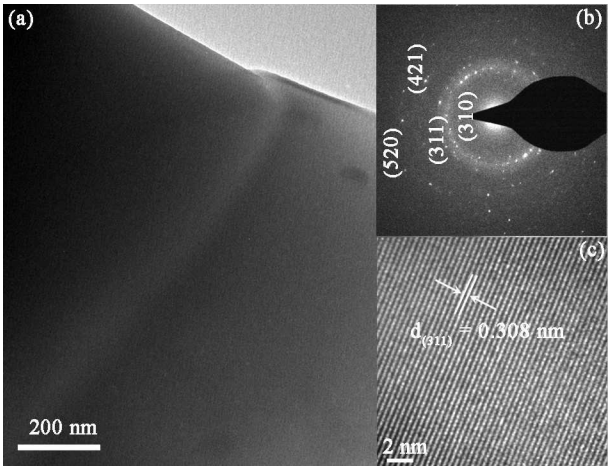

Fig. 2 (a) TEM image of $Ba_2Zr_2Si_3O_{12}$: 0.03Eu^{2+}, (b) corresponding SAED pattern and (c) HRTEM images of the selected area.

to the $4f^7$-$4f^65d^1$ transitions of Eu^{2+} from the ground state to the different splitting levels of the 5d state. [34-36] Under the excitation of 365 nm, the BZSO: 0.03Eu^{2+} phosphor produce very broad asymmetric emission band peaking at around 501 nm with the full-width at half maximum (FWHM) about 3751 cm^{-1}, which corresponds to the typical $4f^65d^1$-$4f^7$ transition of Eu^{2+} ion.[27, 37] The inset of Fig. 3a shows the corresponding CIE chromaticity diagram (0.191, 0.412) and digital photograph for the BZSO: 0.03Eu^{2+} sample monitored at the wavelength of 365 nm, which indicates that this material can be potentially used as a green phosphor for WLEDs. Generally, the electron-vibrational interaction of the Eu^{2+} 5d states is influenced by the following parameters: the Stokes shift ΔE_S, the Huang-Rhys factor S and effective phonon energy $\hbar\omega$.[38-42] In order to facilitate the analysis, the following equations could be applied:

$$\Delta E_S = (2S\text{-}1)\hbar\omega \quad (1)$$

$$\Gamma(T) = 2.35\hbar\omega\left[S\coth\left(\frac{\hbar\omega}{2kT}\right)\right]^{1/2} \quad (2)$$

Taking the Stokes shift as 5292 cm^{-1} and the full-width at half maximum (FWHM) about 3751 cm^{-1}, the value of the Huang–Rhys factor S and effective phonon energy $\hbar\omega$ can be calculated as 3.68 and 832 cm^{-1}, respectively.[38, 39] As is known to all, the energetic position of the 5d-band edges (E) for the Eu^{2+} ion is sensitive to electron-electron repulsion between the center ion and its surrounding anions, which can be estimated from the relation

$$E(cm^{-1}) = Q[1-(\frac{V}{4})^{1/V}\,\mathrm{x}10^{-(nE_a r)/80}] \quad (3)$$

where E is the position of the emission band of rare-earth ions (cm^{-1}), Q is the position in energy for the lower d-band edge of the free ion (34000 cm^{-1} for Eu^{2+}), V is the valence state of the Eu^{2+} ion (V = 2), n is the number of anions in the immediate shell around Eu^{2+} ion, which is the coordination number of Eu^{2+}, E_a is the electron affinity of the anions around the Eu^{2+} ion (in eV), and r is the ionic radius of the host cation replaced by Eu^{2+} (in Å).[38, 43]

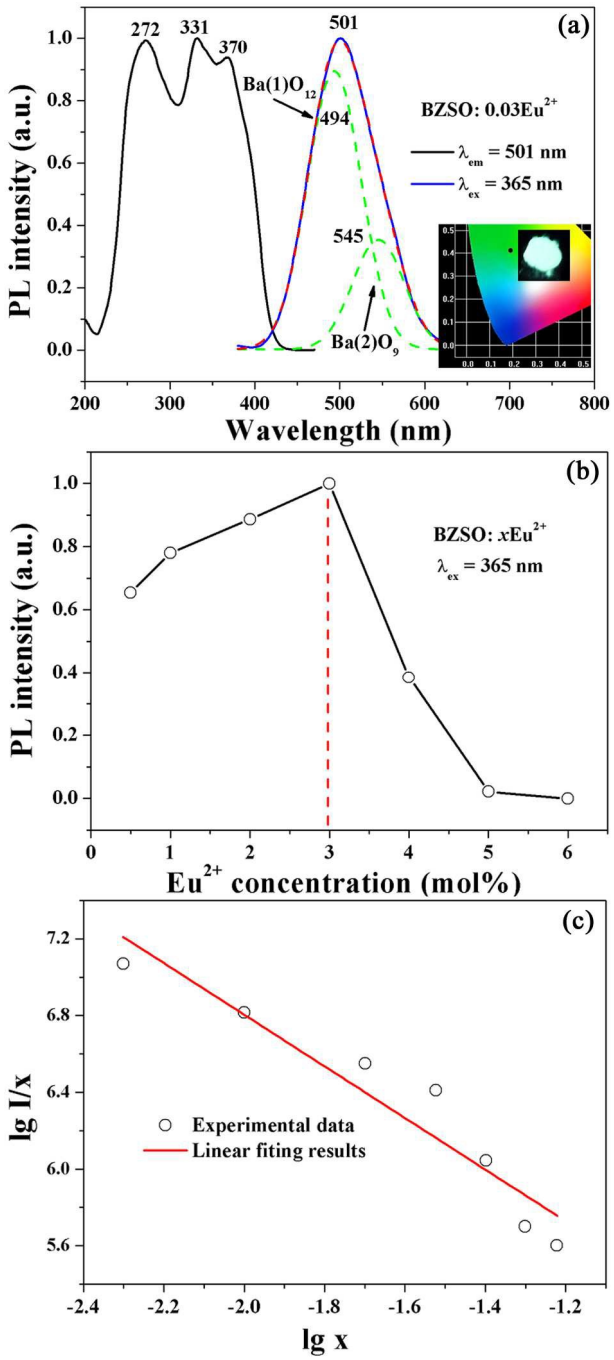

Fig. 3 (a) The PLE and PL spectra of BZSO: 0.03Eu^{2+} sample, (b) The PL intensity of BZSO: xEu^{2+} samples as a function of Eu^{2+} doping concentrations, (c) The plots lg I/x *vs* lg x of the BZSO: xEu^{2+} phosphor, under the excitation of 365 nm.

On the basis of the above analysis, it is apparently that the value of E (cm^{-1}) is directly proportional to the product of n and r. Thus, it is reasonable to assign that the emission bands at 494 nm (20243 cm^{-1}) and 545 nm (18348 cm^{-1}) correspond to Ba(1)O_{12} (CN = 12) and Ba(2)O_9 (CN = 9), respectively, basically agreeing

well with the XRD refinement results.

The influence of doping concentration of Eu^{2+} ions on the emission intensity of the obtained BZSO: $x$$Eu^{2+}$ phosphor is

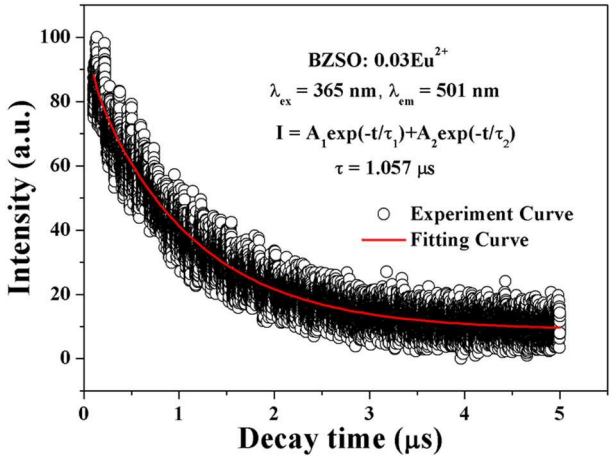

Fig. 4 Decay curves of BZSO: $0.03Eu^{2+}$ sample (λ_{ex} = 365 nm, λ_{em} = 501 nm).

displayed in Fig. 3b. It is apparently that the optimum doping concentration of Eu^{2+} ions is x = 0.03, and beyond this value, the intensity decreases sharply due to the concentration quenching effect. The concentration quenching appears because the spontaneous energy transfers from one activator to another, leading to nonradiative transitions.[44-46] The critical distance R_C between Eu^{2+} ions can be roughly calculated by concentration quenching method using the equation

$$R_C \approx 2\left[3V / 4\pi X_C N\right]^{1/3} \qquad (4)$$

where V is the volume of the unit cell, X_C is the critical concentration of doped ions, and N is the number of the host cations in the unit cell.[47, 48] For BZSO: $0.03Eu^{2+}$, N = 8 and V = 1074.62 Å^3, X_C is 0.03 for Eu^{2+}, therefore, the critical distance (R_C) was calculated to be about 20.45 Å. Since the typical critical distance is about 5 Å for exchange interaction, which is much smaller than the obtained result 20.45 Å, thus, the exchange interaction can be ruled out.[49-51] Therefore, the energy-transfer mechanism is attributed to the interaction of multipolar-multipolar, which can be easily deduced from the following equation

$$\frac{I}{x} = K\left[1+\beta(x)^{\theta/3}\right]^{-1} \qquad (5)$$

where the values of θ are 6, 8 and 10 corresponding to dipole-dipole, dipole-quadrupole and quadrupole-quadrupole interaction, respectively, I is the luminescence intensity, x is the concentration of activator, K and β are the constants for a given excitation wavelength and crystal structure.[52] According to the above analysis, the value of θ in our experiment is approximately equal to 6 after calculation shown in Fig. 3c, which means that the concentration quenching mechanism of BZSO: $x$$Eu^{2+}$ phosphors is dipole–dipole interaction. Furthermore, the R_C could be also obtained through spectra overlap method with the formula

$$R_c^{\,6} = 0.63\text{x}10^{28}\,\frac{4.8\text{x}10^{-16}\cdot P}{E^4}\int f_s(E)f_a(E)dE \quad (6),$$

where E is the energy of maximum spectral overlap, P is oscillator strength of the Eu^{2+} ion (0.01 for an allowed 4f-5d transition) and $\int f_s(E)f_a(E)dE$ is the spectral overlap integral from the normalized excitation and emission spectrum of BZSO: $0.03Eu^{2+}$.[15, 27, 53] The values of E and $\int f_s(E)f_a(E)dE$ were calculated to be 3.05 and 0.85 eV^{-1} from the spectra, respectively. Thus, the R_C was calculated to be 25.83 Å, which is consistent with the result obtained through the concentration quenching method.

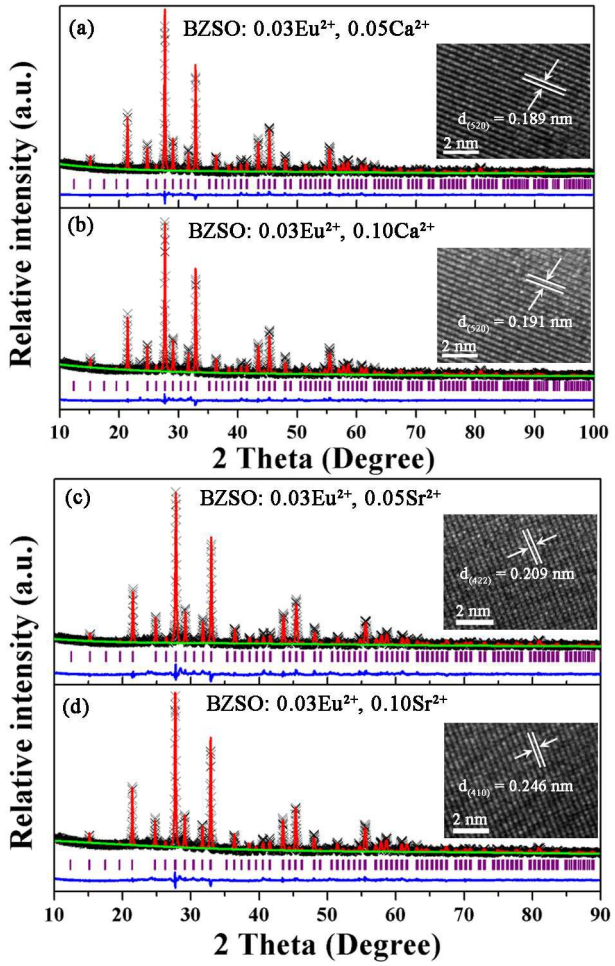

Fig. 5 The Selected Rietveld refinement to XRD patterns for BZSO: $0.03Eu^{2+}$, $m$$Ca^{2+}$ (a) m = 0.05, (b) m = 0.10 and BZSO: $0.03Eu^{2+}$, $n$$Sr^{2+}$ (c) n = 0.05, (d) n = 0.10, respectively. The insets are corresponding HRTEM images.

As displayed in Fig. 4, the decay curves of BZSO: $0.03Eu^{2+}$ could be well fitted to double exponential functions as $I = A_1\exp(-t/\tau_1) + A_2\exp(-t/\tau_2)$, from which the average lifetime of Eu^{2+} ($4f^6 5d^1$-$4f^7$ transition) was calculated to be 1.057 μs.[15, 36] The double exponential decay dynamic is in agreement with the fact that there exist two types of cation sites in the host lattice. The average lifetimes were determined to be 2.091, 1.151, 1.135, 0.965, 0.882, and 0.826 μs for x = 0.005, 0.01, 0.02, 0.04, 0.05 and 0.06 in BZSO: $x$$Eu^{2+}$, respectively. The lifetime decreases in the BZSO: $x$$Eu^{2+}$ system with the increase of Eu^{2+} concentration, which due to the fact that the distance between Eu^{2+} ions shortens

at higher doping content, thus the interactions become stronger.[26]

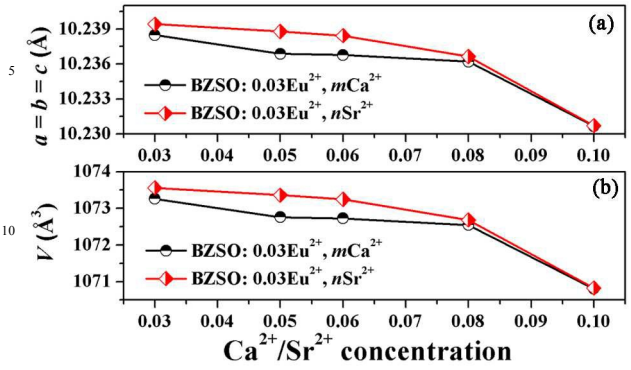

Fig. 6 Unit cell parameters of BZSO: $0.03Eu^{2+}$, Ca^{2+}/Sr^{2+} obtained from Rietveld refinement data present both a contraction in the (a) lattice parameter and (b) cell volume as the concentration of Ca^{2+}/Sr^{2+} increases, reflecting the effects of the cations substitutions.

Although the $4f^65d^1$-$4f^7$ transitions of Eu^{2+} ions have intrinsic characteristics that contribute to the optical properties, these transitions are parity-allowed and sensitive to the crystal fields of the surrounding ions. Thus, this dependence on the crystal field enables tuning of the emission color.[5, 6, 54, 55] By employing isovalent substitutions with varying sizes (Ca^{2+}/Sr^{2+} for Ba^{2+}), we could alter the local environment for Eu^{2+} ions in BZSO: $0.03Eu^{2+}$ and thereby the luminescence properties. Firstly, Rietveld refinement with GSAS program has been performed to obtain more detailed information to investigate how substitution (Ca^{2+}/Sr^{2+} for Ba^{2+}) affects the BZSO: $0.03Eu^{2+}$ crystal structure. As the selected samples shown in Fig. 5, the observed, calculated and the difference results from the refinements are consistent with the Bragg reflections, which indicates the formation of a single phase. The inset HRTEM images present a very uniform contrast, verifying that these single-phase samples are highly crystalline and without significant defects. Table S2 summarizes reliability factors and lattice parameters of BZSO: $0.03Eu^{2+}$, $m Ca^{2+}$ (m = 0.01-0.10) and BZSO: $0.03Eu^{2+}$, $n Sr^{2+}$ (n = 0.01-0.10) samples. In all cases, the structure refinements converged with final R_p about 6% and R_{wp} about 8%, which revealing a good quality of fit. As the lattice parameters for BZSO: $0.03Eu^{2+}$, $m Ca^{2+}$ and BZSO: $0.03Eu^{2+}$, $n Sr^{2+}$ phases determined from Rietveld refinement analysis plotted in panels a and b in Fig. 6, all lattice parameters show smooth evolution and the volumes of lattice decrease with the increasing of contents of Ca^{2+} or Sr^{2+} according to the Vegard's rule, due to the fact that larger Ba^{2+} is substituted by smaller ions of Ca^{2+} and Sr^{2+}.[33, 56] Comparing with the Ca^{2+} series, the Sr^{2+}-doped series have lager lattice parameters and volumes because of the different ionic radii ($r_{Ca} < r_{Sr}$).

Fig. 7 shows the emission spectra of BZSO: $0.03Eu^{2+}$, $m Ca^{2+}$ and BZSO: $0.03Eu^{2+}$, $n Sr^{2+}$, with m and n corresponding to various molar concentrations (0-0.10) of Ca^{2+} and Sr^{2+}, respectively, under the excitation of 365 nm. It is obvious that there is a continuous blue shift from 501 nm to 472 nm for Ca^{2+}-doped and 501 nm to 480 nm for Sr^{2+}-doped samples, respectively. The emission, Stokes shift, centre of gravity, crystal filed splitting and the CIE coordinates for BZSO: $0.03Eu^{2+}$, $m Ca^{2+}$ and BZSO: $0.03Eu^{2+}$, $n Sr^{2+}$ are summarized in Table S3. As shown inset of Fig. 7, the chromaticity coordinates for BZSO: $0.03Eu^{2+}$, $m Ca^{2+}$ and BZSO: $0.03Eu^{2+}$, $n Sr^{2+}$ phosphors can be tuned in the range from (0.191, 0.412) to (0.165, 0.243) and from (0.191, 0.412) to (0.163, 0.274), respectively, which means that the emission color between green and cyan in the visible region of the spectrum can be easily obtained by varying the divalent metal ions, such as: Ca^{2+} or Sr^{2+}, like the photographs of BZSO: $0.03Eu^{2+}$, $0.10Ca^{2+}$ and BZSO: $0.03Eu^{2+}$, $0.10Sr^{2+}$ displayed inset of Fig. 7a and b. The overall tendencies of Stokes shift and emission energy in the BZSO: $0.03Eu^{2+}$, $m Ca^{2+}$ and BZSO: $0.03Eu^{2+}$, $n Sr^{2+}$ systems are plotted in Fig. 8. In summary, the tendency of increase in emission energy with the increasing of m or n is unexpected and contrary to the traditional theory about crystal field strength.[49, 57] Generally, the progressive replacement of Ba^{2+} by smaller Ca^{2+}/Sr^{2+} ions is expected to be followed by shorter metal-ligand distance, resulting a stronger crystal field environment, which can be proved by the decreasing of lattice parameters and volumes shown in Fig. 6, thereby causing red

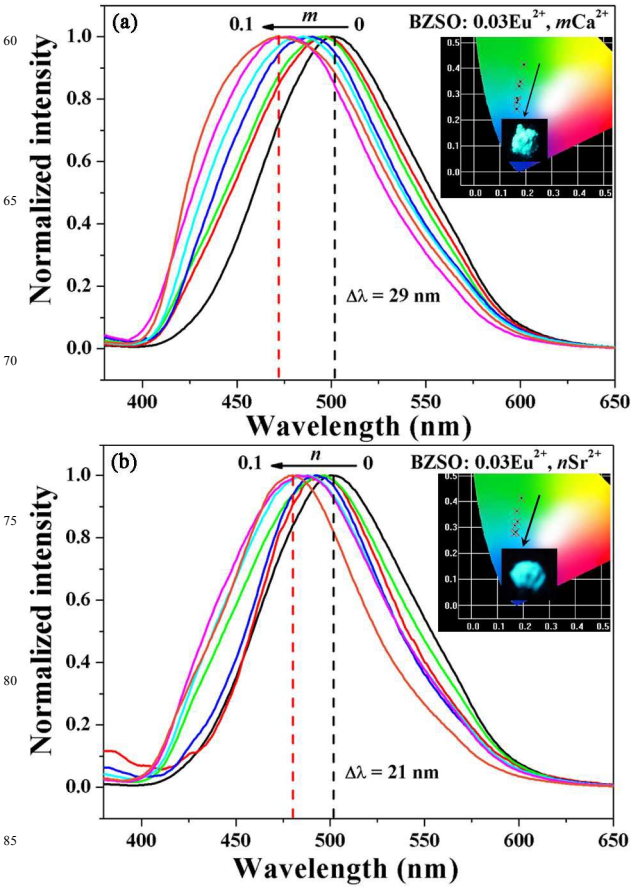

Fig. 7 The variation of emission position of (a) BZSO: $0.03Eu^{2+}$, $m Ca^{2+}$ and (b) BZSO: $0.03Eu^{2+}$, $n Sr^{2+}$ with changing Ca^{2+}/Sr^{2+} concentrations. The inset shows the corresponding CIE chromaticity coordinates and the photographs of BZSO: $0.03Eu^{2+}$, $0.10Ca^{2+}$ and BZSO: $0.03Eu^{2+}$, $0.10Sr^{2+}$, respectively, under 365 nm excitation.

shift in emission, meanwhile, decreasing the emission energy.[43, 58] Such abnormal blue shift emission properties should be clarified

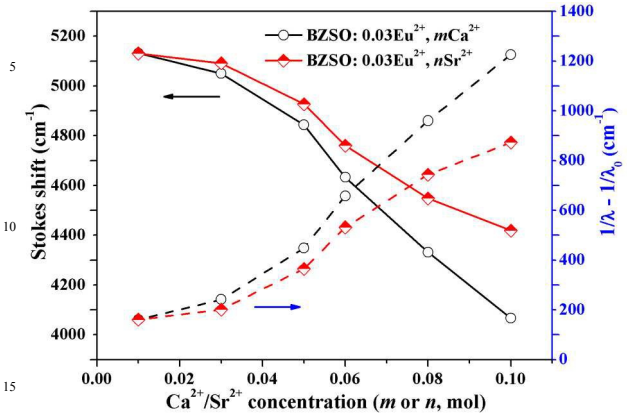

Fig. 8 The overall tendencies of Stokes shift and emission energy in the BZSO: 0.03Eu^{2+}, $m$$Ca^{2+}$ and BZSO: 0.03Eu^{2+}, $n$$Sr^{2+}$ systems are plotted as a function of Ca^{2+}/Sr^{2+} doping concentrations.

in more details. Accordingly, we propose the underlying mechanisms of the differences between the average structure and the local coordination environments on activator ions (Eu^{2+}) for this unusual blue shift emission.

Generally, the luminescence properties of phosphors are influenced by their size and morphology. However, it is obvious that the size and morphology of BZSO: 0.03Eu^{2+} varied little with introduction of Ca^{2+}/Sr^{2+}, as the SEM shown in the Fig. S1, which is ascribed to the high temperature solid state reaction method. Thus, it can be concluded that the variation of the luminescent property is mainly due to the change of local environment around the activator. Firstly, bond valence sums (BVS), shown in Fig. 9, were calculated from refinements of X-ray diffraction data to help determine the microstructure of Ba^{2+} sites.[59, 60] Ba^{2+} on both Ba(1) and Ba(2) sites have comparable BVS, which are under-bonded with a value smaller than +2, while Si^{4+} is highly over-bonded with a value greater than +4. Macroscopically speaking, this structure causes one site to be under-bonded and one site to be over-bonded, which is deleterious to the stability. However, taking into account the refined bond length of Ba-Si and Ba-Zr, it is able to balance this situation and achieve an optimum condition by the formation of subunits of Ba-O-Si due to the fact that the bond length of Ba-Si is smaller than Ba-Zr. Thus, the BVS of these subunits has been calculated as shown in Fig. 9, which is consistent with the optimum value displayed in green line. This means that these subunits help to form a highly rigid substructure, which would have a great influence on the PL properties. To clarify the local environments of Eu^{2+} sites, the effect of Ca^{2+}/Sr^{2+} incorporation involved in the Eu^{2+} activators can be analyzed by the variations of ionic radii and cell volumes, as shown in Fig. 10. It is obvious that the decrease of cell volume is relatively small compared with the decrease of ionic radii with the introduction of Ca^{2+}/Sr^{2+}. Thus, it can be deduced that microenvironment of activators is expanded to some extent so as to compensate for the decrease of ionic radii in comparison with the $Ba_2Zr_2Si_3O_{12}$ host.[61] So, we can conclude that the blue shift of the Eu^{2+} emission with

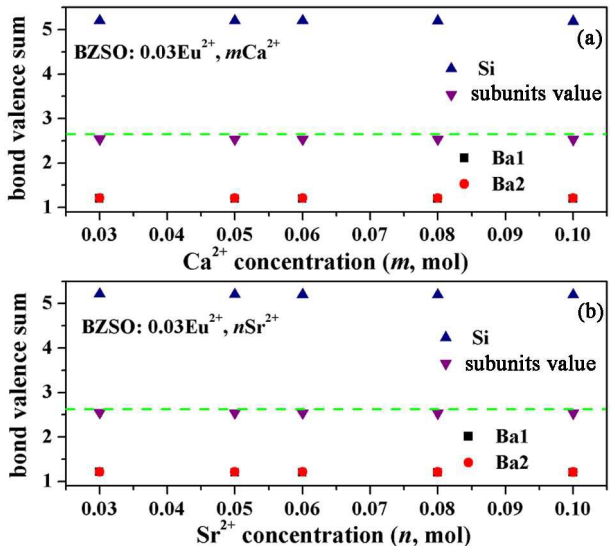

Fig. 9 The bond valence sums (BVS) of Ba(1), Ba(2) and Si atoms in the BZSO: 0.03Eu^{2+}, $m$$Ca^{2+}$ and BZSO: 0.03Eu^{2+}, $n$$Sr^{2+}$ systems. BVS analysis indicates that the formation of Ba-O-Si subunits is an optimal bonding environment for activators.

increasing Ca^{2+}/Sr^{2+} concentrations was ascribed to the decrease of the crystal field strength that the 5d orbital of Eu^{2+} ion experiences due to the differences between the average structure and the local coordination environments on activator ions.[62]

As the introduction of Ca^{2+}/Sr^{2+} ions, the crystal structure of the BZSO: 0.03Eu^{2+} system would change to some extent, thus, the local environment of the Eu^{2+}-substituted sites are significantly changed due to bond-length changes between the activator cation and the ligand anion.[6, 63] According to the equation

$$\Delta = Dq = \frac{Ze^2r^4}{6R^5} \quad (7)$$

where Dq is a measure of the crystal field strength, Z is the charge or valence of the anion, e is the charge of the electron, r is

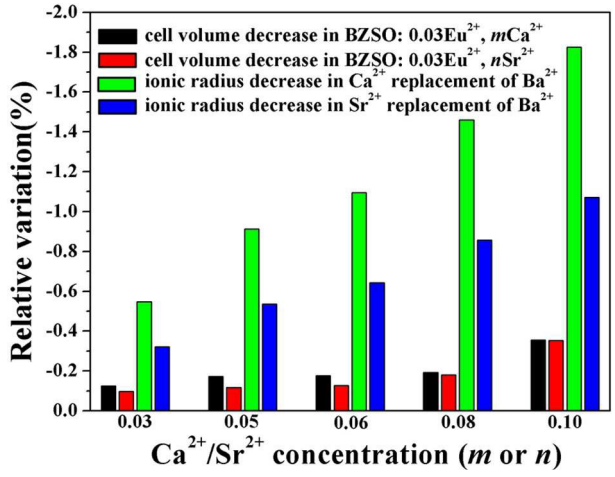

Fig. 10 The variations of cell volumes and ionic radii in the

BZSO: 0.03Eu^{2+}, *m*Ca^{2+} and BZSO: 0.03Eu^{2+}, *n*Sr^{2+} systems.

the radius of the d wavefunction and *R* is the distance between the central ion and its ligands.[64, 65] As discussed above, when Ba^{2+} is substituted by a smaller Ca^{2+} ion, the crystal site of Eu^{2+} is expanded, and the magnitude of the crystal field decreases. Thus, the 5d band of Eu^{2+} is increased and there is a continuous blue shift in the emission along with the increasing of Ca^{2+} content. On the other hand, previous works have shown that the introduction of impurity ions would increase the polyhedral

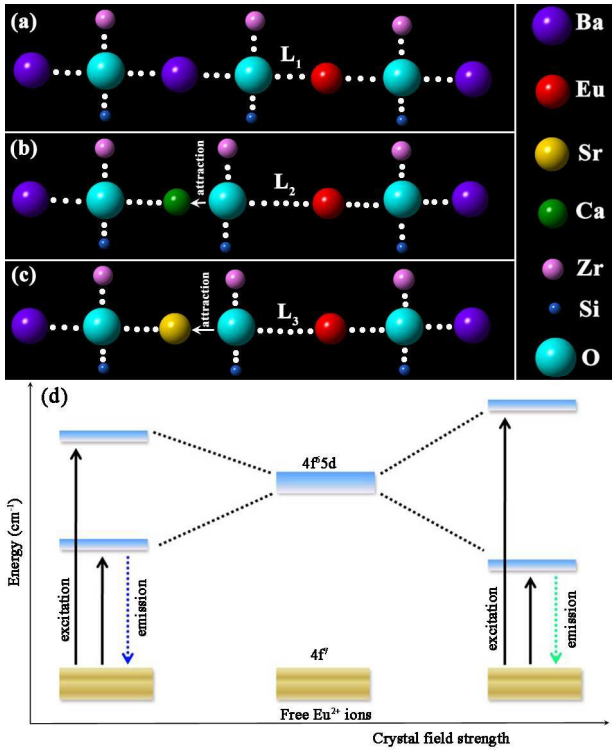

Fig. 11 Local structural coordination of Eu^{2+} ions in host lattices of (a) BZSO: 0.03Eu^{2+}, (b) BZSO: 0.03Eu^{2+}, *m*Ca^{2+} and (c) BZSO: 0.03Eu^{2+}, *n*Sr^{2+} series. (d) The corresponding model for the crystal field strength and emission energy of 5d energy level of Eu^{2+} in strong and weak crystal fields.

distortion index (*D*), which can cause an increased crystal field strength and red shift.[22, 60] However, in our system, the calculated *D* is consistent regardless of the Ca^{2+} concentration, such as 0.0343 for Ba(1) and 0.0401 for Ba(2), based on the equation

$$D = \frac{1}{n}\sum_{i=1}^{n}\frac{|l_i - l_{av}|}{l_{av}} \quad (8)$$

where l_i is the distance from the central atom to the ith coordinating atom and l_{av} is the average bond length, due to the highly rigid substructure of Ba-O-Si subunits as proved above.[22, 66] Therefore, the observed expansion in local environments and consistent distortion index cause weak crystal field strength, thus, resulting blue shift in the PL properties as Ca^{2+} content increases. As for BZSO: 0.03Eu^{2+}, *n*Sr^{2+} system, due to the fact that the radius of Sr^{2+} lies between Ba^{2+} and Ca^{2+}, the crystal field strength is stronger than Ca^{2+} doped samples, thus, the blue shift is smaller compared with the BZSO: 0.03Eu^{2+}, *m*Ca^{2+} system and the similar mechanism will not be discussed in details here. In addition, we have measured the decay curves of BZSO: 0.03Eu^{2+}, *m*Ca^{2+} (*m* = 0.03-0.10) and BZSO: 0.03Eu^{2+}, *n*Sr^{2+} (*n* = 0.03-0.10) samples, and the obtained life times have been listed in the Table S4. The measured decay time is nearly the same, which indicates that they are short enough for potential applications in WLEDs.

As the scheme shown in Fig. 11a, the centre Ba^{2+} ions is surrounded by coordinated O^{2-} ions that also linked with other neighboring cations, such as Si^{4+}, Zr^{4+}, and outer Ba^{2+} ions. Once introduction of activator ion, Eu^{2+} would randomly occupy Ba^{2+} positions in the host lattice, thus, resulting in the green emission. In the BZSO: 0.03Eu^{2+}, *m*Ca^{2+} and BZSO: 0.03Eu^{2+}, *n*Sr^{2+} system, the Ba^{2+} cations are replaced by smaller Ca^{2+} and Sr^{2+} cations at the second-neighbor sites of the Eu^{2+} ions when *m* and *n* increase, which would have a dominant effect on the PL properties. Generally, the ionic potential can be used to evaluate the attractive force of the central cations towards the anions, which can be estimated using the following formula $\varphi = Z/r$ where *Z* is the electric charge number of ion, and *r* is the ion radius (pm).[67] As is known, the ionic radii of Ba^{2+}, Ca^{2+} and Sr^{2+} is in the sequence of $r(Ba^{2+}) > r(Sr^{2+}) > r(Ca^{2+})$, so the $\varphi(Ca^{2+}) > \varphi(Sr^{2+}) > \varphi(Ba^{2+})$. Thus, the Ca^{2+} has the highest attractive force towards O^{2-}, followed by the Sr^{2+} ions. When Ba^{2+} is substituted by a smaller Ca^{2+} ion, the bond length between Eu^{2+} and O^{2-} (L_2) becomes longer and the magnitude of the crystal field strength decreases, thus, resulting in the blue shift in the emission. Considering the circumstance of Sr^{2+}-doped series, the blue shift in the emission is smaller than in the Ca^{2+} series due to the fact that $\varphi(Sr^{2+})$ lies between $\varphi(Ca^{2+})$ and $\varphi(Ba^{2+})$ and L_3 is shorter than L_2, thus the crystal field strength is in the middle. The corresponding models for the crystal field strength and emission energy of 5d energy level of Eu^{2+} are shown in Fig. 11d.

The thermal stability of phosphors is an important index for the practical application of WLEDs.[68, 69] Temperature-dependent of relative emission intensities for BZSO: 0.03Eu^{2+}, BZSO: 0.03Eu^{2+}, 0.05Sr^{2+} and BZSO: 0.03Eu^{2+}, 0.05Ca^{2+} phosphors under 365 nm excitation in the temperature range of 300-500 K is compared in Fig. 12a. It is obvious that the normalized emission intensities of all three samples decrease with increasing of temperature. Taking BZSO: 0.03Eu^{2+} for example, the emission band has a slight blue shift towards higher energy side shown in Fig. 12b. This phenomenon can be ascribed to the thermally active phonon-assisted tunneling from the excited states of the lower-energy emission band to those of the high-energy emission band in the configuration coordinate diagram.[36] A decay of 52% for BZSO: 0.03Eu^{2+}, 47% for BZSO: 0.03Eu^{2+}, 0.05Sr^{2+} and 40% for BZSO: 0.03Eu^{2+}, 0.05Ca^{2+} at 405K was observed, respectively. Comparing with the BZSO: 0.03Eu^{2+}, 0.05Ca^{2+} sample, the emission intensity of BZSO: 0.03Eu^{2+}, 0.05Sr^{2+} decreases much faster with increasing temperature, while slowly than that of BZSO: 0.03Eu^{2+}, which means that the co-doping of Sr^{2+} and Ca^{2+} makes a contribution to the thermal stability. The temperature dependence of the emission intensity is described by a modified Arrhenius equation

$$I_T = \frac{I_0}{1 + A\exp(-\Delta E/kT)} \quad (9)$$

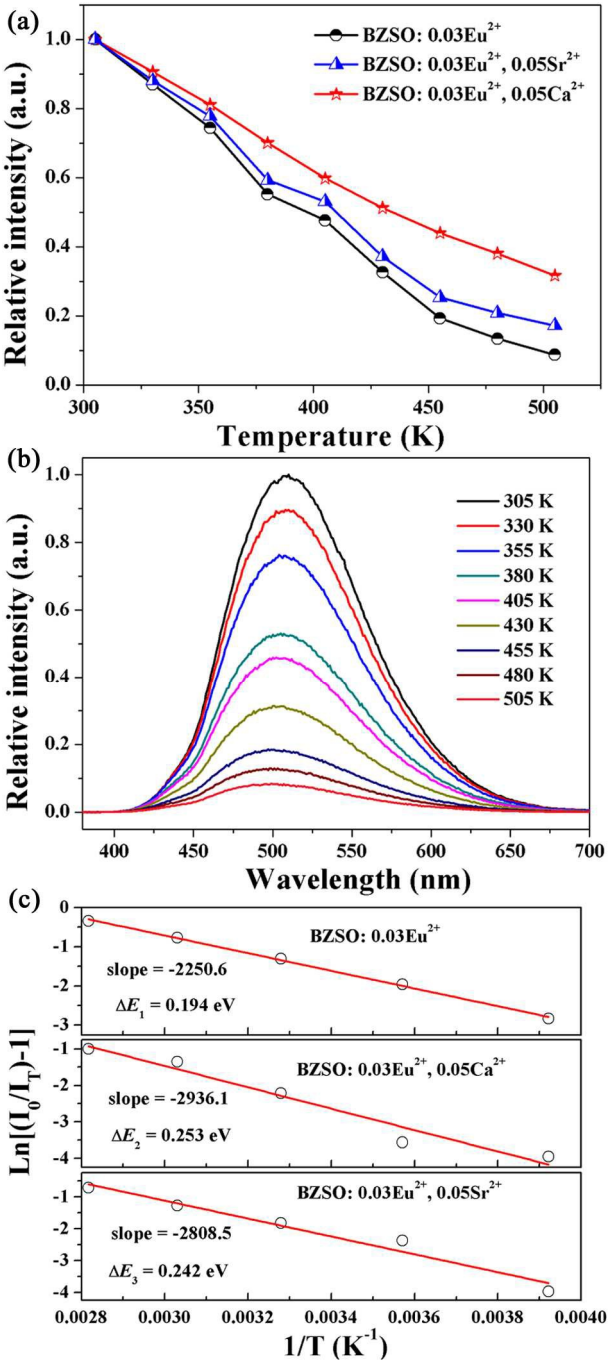

Fig. 12 (a) The variation of PL intensity of BZSO: $0.03Eu^{2+}$, BZSO: $0.03Eu^{2+}$, $0.05Ca^{2+}$ and BZSO: $0.03Eu^{2+}$, $0.05Sr^{2+}$ as a function of temperature and (b) the temperature dependence of emission spectra of BZSO: $0.03Eu^{2+}$ excited at 365 nm. (c) the corresponding activation energy for thermal quenching.

where I_T and I_0 are the intensities of the initial and different temperatures respectively, A is a constant for a certain host, ΔE is the activation energy of thermal quenching and k is the Boltzmann constant (8.617×10^{-5} eV K^{-1}).[34, 70] Fig. 12c plots $\text{Ln}[(I_0/I_T)\text{-}1]$ versus $1/T$ for BZSO: $0.03Eu^{2+}$, BZSO: $0.03Eu^{2+}$, $0.05Ca^{2+}$ and BZSO: $0.03Eu^{2+}$, $0.05Sr^{2+}$ phosphors, respectively. Accordingly, ΔE was calculated to be 0.194 eV (ΔE_1), 0.253 eV (ΔE_2) and 0.242 eV (ΔE_3), respectively. Considering the truth that these samples adopted the same cubic crystal system with space group $P2_13$ (No. 198), the difference in thermal stability is in relation with the change in Stokes shift, which can be explained by the configuration coordinate diagram in Fig. 13.[21, 71] Normally, the total energy of a system is the sum of the ion energy and electron energy. For simplification, the activators (Eu^{2+} for our system) and the corresponding neighbor ions are always selected, ignoring the effects of other ions. The R represents the Stokes shift, which is in close relation with the interatomic distance between the Eu^{2+} and the coordination anions.[6] The ground and the different three excited states of Eu^{2+} can be described with parabolas. After absorption the excitation energy, undesirable

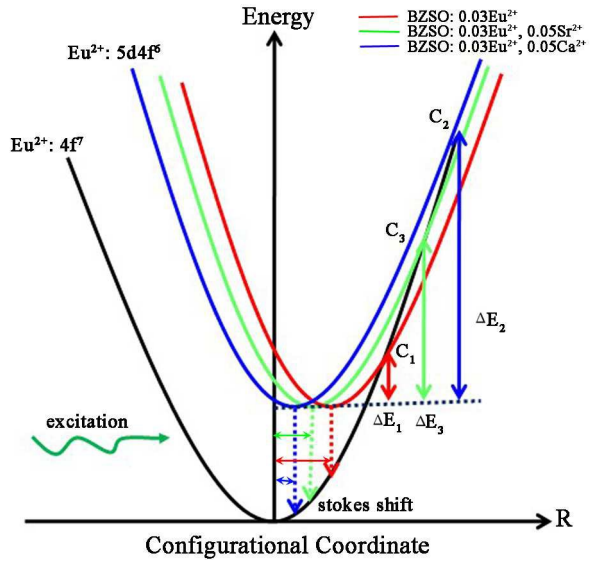

Fig. 13 The configuration coordinate diagram presents the thermal quenching of Eu^{2+} in three different local environments caused by Stokes shift in BZSO: $0.03Eu^{2+}$, BZSO: $0.03Eu^{2+}$, $0.05Ca^{2+}$ and BZSO: $0.03Eu^{2+}$, $0.05Sr^{2+}$.

nonradiative relaxation (phonons) occurs, then emission takes place at the bottom of the excited state by radiative transitions. However, under high temperature, thermal activation can happen due to the electron-phonon coupling and the energy reaches to the crossing point (C) between the excited and ground states.[21, 68] In this case, nonradiative relaxation occurs by heat dissipation rather than radiation emission, which could quench the luminescence. With the decrease in Stokes shift, the thermal activation energy increases in the sequence $\Delta E_2 > \Delta E_3 > \Delta E_1$, which means that smaller Stokes shift results in lower thermal quenching behavior.[21] Therefore, doping of Ca^{2+} and Sr^{2+} is beneficial to improve the thermal stability of BZSO: $0.03Eu^{2+}$ system, especially Ca^{2+} ions.

4. Conclusion

In summary, a bright green-emitting (peaking at 501 nm) $Ba_2Zr_2Si_3O_{12}$: Eu^{2+} phosphor has been developed in a reduced atmosphere using high temperature solid state reaction method, which has a broad excitation band ranging from 200 to 450 nm, matching with the emission of NUV LED chips. The crystal structure of BZSO: Eu^{2+} was determined by the Rietveld refinement analysis. The energy transfer among the Eu^{2+} ions has been proved to be via a dipole–dipole mechanism, and the critical distance (R_C) for Eu^{2+} ions calculated by the concentration quenching and spectral overlap methods are 20.45 and 25.83 Å, respectively. In addition, through the replacement of Ba^{2+} by smaller Ca^{2+} and Sr^{2+}, the overall blue shift in emission (from green to cyan) and increase in quenching barrier height take place due to the decrease of crystal field strength caused by the differences between the average structure and the local coordination environments on activator ions (Eu^{2+}) confirmed by the refinement results. This research not only unveils the relations of composition-structure-property, but also may serve as a guideline for developing tunable luminescence in single-phased materials.

Acknowledgements

This project is financially supported by National Natural Science Foundation of China (Grants NSFC 91433110，51172227, 51472234), the National Basic Research Program of China (Grants 2014CB643803), and the Joint Funds of the National Natural Science Foundation of China and Guangdong Province (Grant No. U1301242)

Notes and references

[a] *State Key Laboratory of Rare Earth Resource Utilization, Changchun Institute of Applied Chemistry, Chinese Academy of Sciences, Changchun, 130022,P. R. China. E-mail: jlin@ciac.ac.cn; Tel: +86-431-85262031*

[b] *University of the Chinese Academy of Sciences, Beijing 100049, P. R. China*

†Electronic Supplementary Information (ESI) available: The SEM images of (a) BZSO: 0.03Eu^{2+}, (b) BZSO: 0.03Eu^{2+}, 0.10Ca^{2+}, (c) BZSO: 0.03Eu^{2+}, 0.10Sr^{2+}; Crystallographic data of $Ba_2Zr_2Si_3O_{12}$: 0.03Eu^{2+}, as determined by the Rietveld refinement of power XRD data at room temperature; Crystallographic data and reliability factor of BZSO: 0.03Eu^{2+}, $m$$Ca^{2+}$ (m = 0.03−0.10) and BZSO: 0.03Eu^{2+}, $n$$Sr^{2+}$ (n = 0.03−0.10) materials; Excitation, emission, centre of gravity, Stokes shift and crystal filed splitting and the CIE coordinates of of BZSO: 0.03Eu^{2+}, $m$$Ca^{2+}$/$n$$Sr^{2+}$; The decay life times of Eu^{2+} in BZSO: 0.03Eu^{2+}, $m$$Ca^{2+}$ (m = 0.03−0.10) and BZSO: 0.03Eu^{2+}, $n$$Sr^{2+}$ (n = 0.03−0.10) materials. See DOI: 10.1039/b000000x/

1. E. Matioli, S. Brinkley, K. M. Kelchner, Y.-L. Hu, S. Nakamura, S. DenBaars, J. Speck and C. Weisbuch, *Light Sci. Appl.*, 2012, **1**, e22.
2. J. H. Oh, S. J. Yang and Y. R. Do, *Light Sci. Appl.*, 2014, **3**, e141.
3. S. Ye, F. Xiao, Y. X. Pan, Y. Y. Ma and Q. Y. Zhang, *Mater. Sci. Eng., R*, 2010, **71**, 1-34.
4. H. A. Höppe, *Angew. Chem. Int. Ed.*, 2009, **48**, 3572-3582.
5. N. C. George, K. A. Denault and R. Seshadri, *Annu. Rev. Mater. Res.*, 2013, **43**, 481-501.
6. J. McKittrick and L. E. Shea-Rohwer, *J. Am. Ceram. Soc.*, 2014, **97**, 1327-1352.
7. W.-T. Chen, H.-S. Sheu, R.-S. Liu and J. P. Attfield, *J. Am. Chem. Soc.*, 2012, **134**, 8022-8025.
8. R. J. Xie, *J. Am. Ceram. Soc.*, 2013, **96**, 665-687.
9. F. Hintze, F. Hummel, P. J. Schmidt, D. Wiechert and W. Schnick, *Chem. Mater.*, 2011, **24**, 402-407.
10. G. Lozano, D. J. Louwers, S. R. K. Rodriguez, S. Murai, O. T. A. Jansen, M. A. Verschuuren and J. Gomez Rivas, *Light Sci. Appl.*, 2013, **2**, e66.
11. C. C. Lin and R.-S. Liu, *J. Phys. Chem. Lett.*, 2011, **2**, 1268-1277.
12. W. B. Im, N. George, J. Kurzman, S. Brinkley, A. Mikhailovsky, J. Hu, B. F. Chmelka, S. P. DenBaars and R. Seshadri, *Adv. Mater.*, 2011, **23**, 2300-2305.
13. Y. Zhang, D. Geng, X. Li, J. Fan, K. Li, H. Lian, M. Shang and J. Lin, *J. Phys. Chem. C*, 2014, **118**, 17983-17991.
14. H. Zhu, C. C. Lin, W. Luo, S. Shu, Z. Liu, Y. Liu, J. Kong, E. Ma, Y. Cao, R.-S. Liu and X. Chen, *Nat Commun*, 2014, **5**, 4312.
15. S. J. Gwak, P. Arunkumar and W. B. Im, *J. Phys. Chem. C*, 2014, **118**, 2686-2692.
16. C.-H. Huang, T.-S. Chan, W.-R. Liu, D. Wang, Y.-C. Chiu, Y.-T. Yeh and T.-M. Chen, *J. Mater. Chem.*, 2012, **22**, 20210-20216.
17. V. A. Morozov, A. Bertha, K. W. Meert, S. Van Rompaey, D. Batuk, G. T. Martinez, S. Van Aert, P. F. Smet, M. V. Raskina, D. Poelman, A. M. Abakumov and J. Hadermann, *Chem. Mater.*, 2013, **25**, 4387-4395.
18. M. Shang, C. Li and J. Lin, *Chem. Soc. Rev.*, 2014, **43**, 1372-1386.
19. X. Li, J. D. Budai, F. Liu, J. Y. Howe, J. Zhang, X.-J. Wang, Z. Gu, C. Sun, R. S. Meltzer and Z. Pan, *Light Sci. Appl.*, 2013, **2**, e50.
20. M. Seibald, T. Rosenthal, O. Oeckler, F. Fahrnbauer, A. Tücks, P. J. Schmidt and W. Schnick, *Chem. Eur. J.*, 2012, **18**, 13446-13452.
21. G. Li, C. C. Lin, W.-T. Chen, M. S. Molokeev, V. V. Atuchin, C.-Y. Chiang, W. Zhou, C.-W. Wang, W.-H. Li, H.-S. Sheu, T.-S. Chan, C. Ma and R.-S. Liu, *Chem. Mater.*, 2014, **26**, 2991-3001.
22. K. A. Denault, J. Brgoch, M. W. Gaultois, A. Mikhailovsky, R. Petry, H. Winkler, S. P. DenBaars and R. Seshadri, *Chem. Mater.*, 2014, **26**, 2275-2282.
23. H. Nersisyan, H. I. Won and C. W. Won, *Chem. Commun.*, 2011, **47**, 11897-11899.
24. J. Park, S. J. Lee and Y. J. Kim, *Cryst. Growth Des.*, 2013, **13**, 5204-5210.
25. Y. Liu, X. Zhang, Z. Hao, X. Wang and J. Zhang, *Chem. Commun.*, 2011, **47**, 10677-10679.
26. G.-y. Lee, J. Y. Han, W. B. Im, S. H. Cheong and D. Y. Jeon, *Inorg. Chem.*, 2012, **51**, 10688-10694.
27. D.-Y. Wang, C.-H. Huang, Y.-C. Wu and T.-M. Chen, *J. Mater. Chem.*, 2011, **21**, 10818-10822.
28. M. Percival, W. Schmahl and E. Salje, *Phys. Chem. Miner.*, 1989, **16**, 569-575.

29. V. Tomkute, A. Katelnikovas, H. Bettentrup, A. Kareiva and T. Jüstel, *Opt. Mater.*, 2011, **33**, 1272-1277.
30. D.-Y. Wang, L.-L. Wang, T.-J. Lee, T.-M. Chen and B.-M. Cheng, *J. Electrochem. Soc.*, 2011, **158**, J377-J382.
31. A. Larson and R. Von Dreele, *Los Alamos, New Mexico, USA*, 1994, 86-748.
32. C. Seances, *Acad. Sci.,Ser. C* 1980, **276**, 1973-1974.
33. R. D. Shannon, *Acta Crystallogr. Sec. A*, 1976, **32**, 751-767.
34. Z. Xia, X. Wang, Y. Wang, L. Liao and X. Jing, *Inorg. Chem.*, 2011, **50**, 10134-10142.
35. H. Xie, J. Lu, Y. Guan, Y. Huang, D. Wei and H. J. Seo, *Inorg. Chem.*, 2014, **53**, 827-834.
36. Z. Zhao, Z. Yang, Y. Shi, C. Wang, B. Liu, G. Zhu and Y. Wang, *J. Mater. Chem. C*, 2013, **1**, 1407-1412.
37. F. Hintze, N. W. Johnson, M. Seibald, D. Muir, A. Moewes and W. Schnick, *Chem. Mater.*, 2013, **25**, 4044-4052.
38. P. Dorenbos, *J. Lumin.*, 2003, **104**, 239-260.
39. Y. Wang, M. G. Brik, P. Dorenbos, Y. Huang, Y. Tao and H. Liang, *J. Phys. Chem. C*, 2014, **118**, 7002-7009.
40. W. B. Im, S. Brinkley, J. Hu, A. Mikhailovsky, S. P. DenBaars and R. Seshadri, *Chem. Mater.*, 2010, **22**, 2842-2849.
41. D. Zhai, L. Ning, Y. Huang and G. Liu, *J. Phys. Chem. C*, 2014, **118**, 16051-16059.
42. T.-G. Kim, T. Kim, J. Kim, S.-J. Kim and S.-J. Im, *J. Phys. Chem. C*, 2014, **118**, 12428-12435.
43. W.-R. Liu, C.-W. Yeh, C.-H. Huang, C. C. Lin, Y.-C. Chiu, Y.-T. Yeh and R.-S. Liu, *J. Mater. Chem.*, 2011, **21**, 3740-3744.
44. D. L. Dexter and J. H. Schulman, *J. Chem. Phys.*, 1954, **22**, 1063-1070.
45. Y. Zhang, G. Li, D. Geng, M. Shang, C. Peng and J. Lin, *Inorg. Chem.*, 2012, **51**, 11655-11664.
46. W. Zheng, S. Zhou, Z. Chen, P. Hu, Y. Liu, D. Tu, H. Zhu, R. Li, M. Huang and X. Chen, *Angew. Chem. Int. Ed.,* 2013, **125**, 6803-6808.
47. Y. Zhang, D. Geng, X. Kang, M. Shang, Y. Wu, X. Li, H. Lian, Z. Cheng and J. Lin, *Inorg. Chem.*, 2013, **52**, 12986-12994.
48. W.-Y. Huang, F. Yoshimura, K. Ueda, Y. Shimomura, H.-S. Sheu, T.-S. Chan, C.-Y. Chiang, W. Zhou and R.-S. Liu, *Chem. Mater.*, 2014, **26**, 2075-2085.
49. Y. Zhang, D. Geng, M. Shang, Y. Wu, X. Li, H. Lian, Z. Cheng and J. Lin, *Eur. J. Inorg. Chem.*, 2013, **2013**, 4389-4397.
50. L. Van Uitert, *J. Electrochem. Soc.*, 1967, **114**, 1048-1053.
51. R. Reisfeld and L. Boehm, *J. Solid State Chem.*, 1972, **4**, 417-424.
52. Y. Zhang, Z. Wu, D. Geng, X. Kang, M. Shang, X. Li, H. Lian, Z. Cheng and J. Lin, *Adv. Funct. Mater.*, 2014, **24**, 6581-6593.
53. L. G. Van Uitert, *J. Lumin.*, 1984, **29**, 1-9.
54. Bachmann, V.; Ronda, C.; Oeckler, O.; Schnick, W.; Meijerink, A., *Chem. Mater.* 2008, **21**, 316-325.
55. D. Tu, Y. Liu, H. Zhu, R. Li, L. Liu and X. Chen, *Angew. Chem. Int. Ed.,* 2013, **52**, 1128-1133.
56. K. W. Huang, W. T. Chen, C. I. Chu, S. F. Hu, H. S. Sheu, B. M. Cheng, J. M. Chen and R. S. Liu, *Chem. Mater.*, 2012, **24**, 2220-2227.
57. Y.-C. Wu, Y.-C. Chen, T.-M. Chen, C.-S. Lee, K.-J. Chen and H.-C. Kuo, *J. Mater. Chem.*, 2012, **22**, 8048-8056.
58. W. B. Im, N. N. Fellows, S. P. DenBaars, R. Seshadri and Y. I. Kim, *Chem. Mater.*, 2009, **21**, 2957-2966.
59. N. Brese and M. O'keeffe, *Acta Crystallog. Sect. B: Struct. Sci.*, 1991, **47**, 192-197.
60. K. Denault, S. Paden, S. Brinkley, A. A. Mikhailovsky, J. C. Neuefeind, S. P. DenBaars and R. Seshadri, *J. Mater. Chem.*, 2012, **22**, 18204-18213.
61. C.-H. Huang, P.-J. Wu, J.-F. Lee and T.-M. Chen, *J. Mater. Chem.*, 2011, **21**, 10489-10495.
62. N. C. George, A. J. Pell, G. Dantelle, K. Page, A. Llobet, M. Balasubramanian, G. Pintacuda, B. F. Chmelka and R. Seshadri, *Chem. Mater.*, 2013, **25**, 3979-3995.
63. W. B. Park, S. P. Singh and K.-S. Sohn, *J. Am. Chem. Soc.*, 2014, **136**, 2363-2373.
64. J. Y. Han, W. B. Im, D. Kim, S. H. Cheong, G.-y. Lee and D. Y. Jeon, *J. Mater. Chem.*, 2012, **22**, 5374-5381.
65. P. D. Rack and P. H. Holloway, *Mater. Sci. Eng., R.*, 1998, **21**, 171-219.
66. W. Baur, *Acta Crystallog. Sect. B*, 1974, **30**, 1195-1215.
67. L. Lin, X. Sun, Y. Jiang and Y. He, *Nanoscale*, 2013, **5**, 12518-12531.
68. P. Dorenbos, *J. Phys. Cond. Matter*, 2005, **17**, 8103.
69. C.-W. Yeh, W.-T. Chen, R.-S. Liu, S.-F. Hu, H.-S. Sheu, J.-M. Chen and H. T. Hintzen, *J. Am. Chem. Soc.*, 2012, **134**, 14108-14117.
70. W.-R. Liu, C.-H. Huang, C.-W. Yeh, J.-C. Tsai, Y.-C. Chiu, Y.-T. Yeh and R.-S. Liu, *Inorg. Chem.*, 2012, **51**, 9636-9641.
71. Z. Ci, M. Que, Y. Shi, G. Zhu and Y. Wang, *Inorg. Chem.*, 2014, **53**, 2195-2199.

TOC

Tunable luminescence (from green to cyan) and the increased thermal stability have been obtained in BZSO: Eu^{2+} system through the cation substitutions of Ca^{2+}/Sr^{2+} for Ba^{2+}.